Photothermal Engineering of Graphene Plasmons

Renwen Yu, Qiushi Guo, Fengnian Xia, and F. Javier García de Abajo

Phys. Rev. Lett. **121**, 057404 — Published 2 August 2018

DOI: 10.1103/PhysRevLett.121.057404

Photothermal Engineering of Graphene Plasmons

Renwen Yu,[1] Qiushi Guo,[2] Fengnian Xia,[2] and F. Javier García de Abajo[1,3,*]

[1] *ICFO-Institut de Ciencies Fotoniques, The Barcelona Institute of Science and Technology, 08860 Castelldefels (Barcelona), Spain*
[2] *Department of Electrical Engineering, Yale University, New Haven, Connecticut 06511, USA*
[3] *ICREA-Institució Catalana de Recerca i Estudis Avançats, Passeig Lluís Companys 23, 08010 Barcelona, Spain*

(Dated: June 25, 2018)

Nanoscale photothermal sources find important applications in theranostics, imaging, and catalysis. In this context, graphene offers a unique suite of optical, electrical, and thermal properties, which we exploit to show self-consistent active photothermal modulation of its nanoscale response. In particular, we predict the existence of plasmons confined to the optical landscape tailored by continuous-wave external-light pumping of homogeneous graphene. This result relies on the high electron temperatures achievable in optically pumped clean graphene while its lattice remains near ambient temperature. Our study opens a new avenue toward the active optical control of the nanophotonic response in graphene with potential application in photothermal devices.

PACS numbers: 78.67.-n,65.80.Ck,78.20.Nv,73.20.Mf

Heat deposition via light absorption in nanostructures constitutes a useful tool for controlling nanoscale thermal sources [1–3], with potential application in photothermal therapy [4–6], nanoimaging [7, 8], nanocatalysis [9], data storage [10], and hot-electron devices [11]. Importantly, plasmons in metallic nanostructures enable resonant enhancement of photothermal effects, which can be manipulated down to the nanometer scale [1–3]. Recently, highly doped graphene has emerged as an outstanding two-dimensional material capable of supporting extremely confined surface plasmons that can be actively tuned by varying its Fermi energy through electrical gating and chemical doping [12–25], with application in optical modulation [23, 26–29], light detection [17, 21, 30–33], and sensing [34–36]. Additionally, the photothermal response of graphene is particularly appealing because of the combination of the following three properties: (i) the low number of electrons needed to sustain plasmons in this material compared with conventional three-dimensional metallic structures; (ii) its low electronic heat capacity; and (iii) the strong variation of its optical response produced by electronic heating. Properties (i) and (ii) lead to unusually high electron temperatures under resonant pumping conditions [25, 37, 38], while properties (ii) and (iii), which originate in the conical electronic bands of graphene [25], give rise to an extraordinary photothermal response.

Due to the generally weak electron-phonon coupling in graphene, the electron temperature can reach significantly high values above the lattice background [37, 39]. However, electron-phonon coupling has a dramatic dependence on material quality: in exfoliated clean samples, it is extremely weak and characterized by a relaxation rate that depends linearly on electron-temperature; in contrast, more disordered CVD graphene samples are characterized by a higher relaxation rate with a cubic dependence on electron temperature. The possibility of spatially patterning the electron temperature to manipulate the optical response of graphene appears as a potentially useful approach that deserves further investigation.

In this Letter, we theoretically investigate the photothermally induced optical response of graphene and reveal a radically different behavior in clean and disordered layers leading to unprecedented plasmonic behavior. More precisely, we account in a self-consistent manner for the interplay between optical absorption, heat dissipation, and spatial modification of the electron temperature and optical conductivity under attainable continuous-wave (CW) illumination, and find that weak electron-phonon coupling in clean graphene results in high electron temperatures, while the lattice stays near the ambient level. We exploit this effect to predict (1) a dramatic photothermal modulation of plasmons in graphene ribbons and (2) the existence of plasmons that couple efficiently to external light in homogeneous extended graphene by photothermally patterning a periodic modulation of the optical response. The use of clean graphene samples makes it easier to generate a highly thermalized electron gas under attainable impinging light intensity compared with disordered samples, thus inducing a self-consistent photothermal modulation of plasmons supported in graphene ribbons and creating a channel to excite plasmons even in unstructured graphene sheets. These results illustrate the potential of photothermal engineering to control the plasmonic properties of both structured and extended graphene.

We adopt the local random-phase approximation (local-RPA) to describe the temperature-dependent optical conductivity of graphene $\sigma(\omega)$ [25, 38, 40, 41], combined with a two-temperature model [42] to characterize the position-dependent electron and lattice temperatures (T_e and T_l) under CW illumination in the steady-

state regime of heat dissipation (see details in Supplemental Material, SM [43]). The model incorporates the 2D in-plane thermal electron and lattice conductivities (κ_e and κ_l, obtained from their bulk counterparts by multiplying by the graphene thickness $t = 0.33\,\text{nm}$) to self-consistently calculate the temperature spatial distributions, which are imprinted on the optical conductivity σ through its dependence on T_e [25, 38, 40, 41]. Electron-phonon coupling is accounted for by a power-density coupling $g\,(T_e - T_l)$ for clean graphene and $A\,(T_e^3 - T_l^3)$ for disordered graphene [44–48], where g and A are material-quality-dependent constant coefficients. Additionally, we phenomenologically introduce thermal coupling from the graphene lattice to the substrate through a term $G\,(T_l - T_0)$, where G is a thermal boundary conductance and T_0 is the ambient temperature. In our simulations, we take $T_0 = 300\,\text{K}$ and assume parameter values consistent with reported measurements (see SM [43] for further details): $g \sim 10^4\,\text{W/m}^2\text{K}$, $A = 2.24\,\text{W/m}^2\text{K}^3$, and $G = 5\,\text{MW/m}^2\text{K}$ [49–51]; $\kappa_l/t = 100\,\text{W/mK}$ [52, 53]; and $\kappa_e = 0.1\kappa_l$ [54]. Specific values for the Fermi energy E_F and the E_F-dependent coefficient g are given in the figure captions. Regarding optical damping, we assume a conservative inelastic scattering time $\tau = 66\,\text{fs}$ ($\hbar\tau^{-1} = 10\,\text{meV}$) in both clean and disordered graphene. Although higher τ's have been observed in clean graphene at low temperatures [55, 56], it varies with temperature [57] and our assumed value is realistic when considering high electron temperatures. We use a finite-element method for the latter and iterate the electromagnetic and thermal solutions until self-consistency is achieved typically after ~ 10 iterations. We consider graphene either supported or embedded in an isotropic dielectric of permittivity $\epsilon_h = 4.4$.

We first study a graphene ribbon (width $W = 300\,\text{nm}$) under normal-incidence illumination with transversal polarization [inset to Fig. 1(a)]. A prominent plasmon is observed in the absorption spectrum of Fig. 1(a) for low light intensity (dashed curve). The spectrum remains nearly unchanged at high intensity ($I^{inc} = 100\,\text{MW/m}^2$) in disordered graphene (red solid curve), whereas the plasmon peak undergoes a $\sim$ 10% redshift in clean graphene (blue solid curve). We attribute this different behavior to the much weaker electron-phonon coupling in clean graphene [48], which leads to an elevated electron temperature $T_e \sim 1400\,\text{K}$, in stark contrast to the mild increase in T_e for disorder graphene, as shown in Fig. 1(b).

When varying the incident light intensity in the I^{inc} =1-100 MW/m^2 range, we find a systematic redshift and broadening of the absorption peak in the clean graphene ribbon (Fig. 2). Further increase in intensity up to $200\,\text{MW/m}^2$ produces a large distortion in the absorption spectrum, resulting from the non-monotonic temperature dependence of both the graphene conductivity and the resulting transverse ribbon plasmon energy (see Fig. S1 in SM [43]). The latter admits the analytical expression [25] $\hbar\omega_p = (e/\sqrt{-\pi\eta_1\epsilon_h})\sqrt{\mu^D/W}$, where $\eta_1 = -0.0687$ is an eigenvalue corresponding to the lowest-order dipolar transverse plasmon, while $\mu^D = \mu + 2k_BT_e\log\left(1 + e^{-\mu/k_BT_e}\right)$ and $\mu = E_F\left[\left(1+\xi^4\right)^{1/2} - \xi^2\right]^{1/2}$, with $\xi = (2\log^2 4)(k_BT_e/E_F)^2$, are the temperature-corrected Drude weight and chemical potential, respectively [38]. This expression [solid curve in the inset to Fig. 2(a)] is in excellent agreement with the computed spectral peaks (symbols) when us-

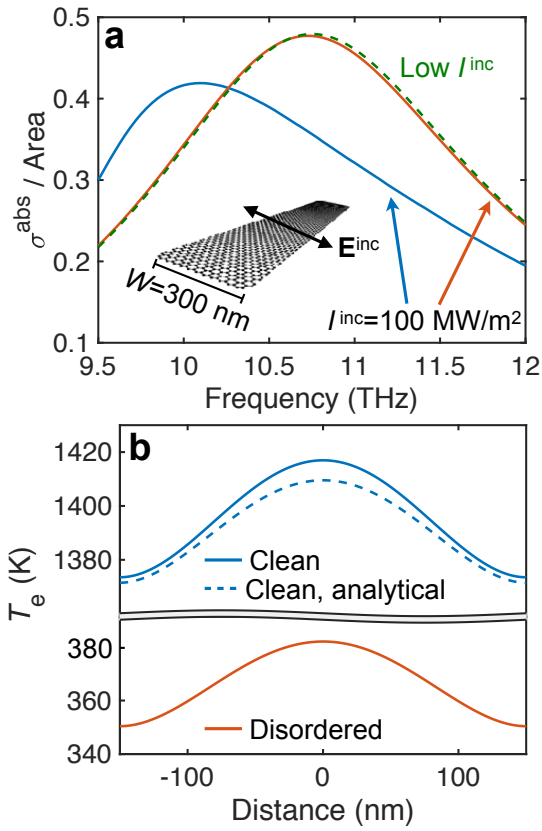

FIG. 1: Plasmon photothermal effect in a graphene ribbon. (a) Normalized normal-incidence absorption cross-section spectra at the spectral peak for a nanoribbon (width $W = 300\,\text{nm}$, $E_F = 0.4\,\text{eV}$, $g = 3.84 \times 10^4\,\text{W/m}^2\text{K}$, embedded in $\epsilon_h = 4.4$) made of either clean or disordered graphene (solid curves), based on a self-consistent description of heat dissipation for an incident light intensity $I^{inc} = 100\,\text{MW/m}^2$. We show results in the low I^{inc} limit for comparison (dashed curve, obtained analytically [41, 58, 59], see SM [43]). (b) Variation of the electron temperature across the ribbon for clean and disordered graphene. We find the lattice temperature to be close to the assumed ambient value of 300 K (see SM [43]). Clean graphene reaches higher electron temperature than disordered graphene because it has a much weaker electron-photon coupling. We describe graphene using the temperature-dependent local-RPA conductivity [25] with a phenomenological inelastic lifetime $\tau = 66\,\text{fs}$ ($\hbar\tau^{-1} = 10\,\text{meV}$). Thermal parameters are given in the main text.

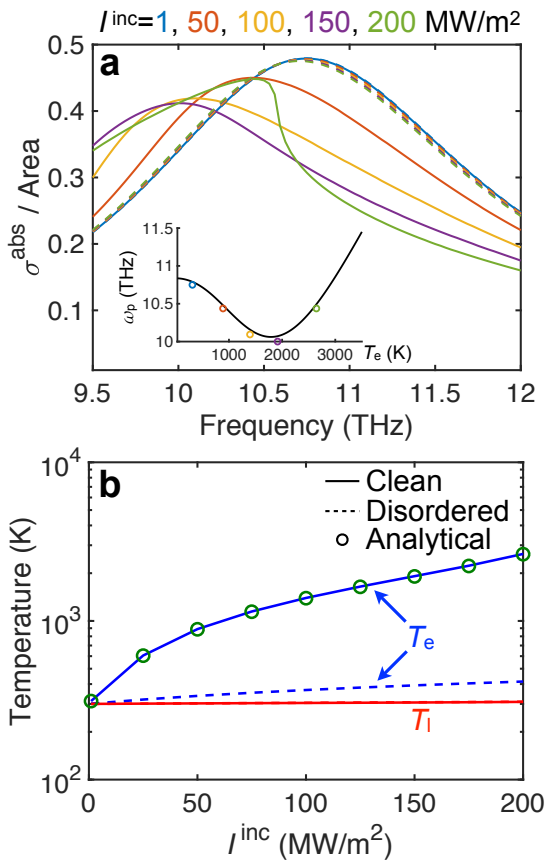

FIG. 2: Light-intensity dependence of the plasmon photothermal effect. (a) Absorption spectra of the graphene nanoribbon considered in Fig. 1 for a wide selection of light intensities. The spectra are dominated by the lowest-order transverse plasmon, the frequency of which is shown in the inset as a function of electron temperature. (b) Space-averaged temperatures (lattice T_l and electrons T_e) as a function of light intensity at the absorption peak frequencies of (a). We present results for both clean (solid curves) and disordered (dashed curves) graphene. Electron-photon coupling is much weaker in clean graphene, leading to higher electron temperatures.

ing the calculated spaced-averaged values of T_e as input. Note that the non-monotonic temperature dependence of the spectral peaks is solely inherited from the temperature dependence of the Drude weight (see explicit expression above), which undergoes a reduction (increase) with increasing temperature when $k_\mathrm{B}T_\mathrm{e} \ll \mu$ ($k_\mathrm{B}T_\mathrm{e} \gg \mu$) [38]. Interestingly, the plasmon FWHM is smaller for $I^\mathrm{inc} = 200\,\mathrm{MW/m^2}$ than for dimmed illumination (Figs. 1 and S2 in SM [43]).

Remarkably, under these attainable conditions, the electrons reach a temperature above 2500 K in clean graphene, while the lattice remains near the ambient level [Fig. 2(b)]. We stress again that this is in stark contrast to disordered graphene, for which the spectra remain nearly unchanged within the considered intensity range and the electron temperature hardly exceeds 400 K (Fig. 2(b) and Fig. S3 in SM [43]) due to a more efficient electron-phonon coupling.

We obtain further insight into the photothermal response of clean graphene by adopting the reasonable assumption $T_\mathrm{l} \approx T_0$, which effectively decouples the lattice from the electronic system (see Figs. S3-S5 in SM [43]), so that heat dissipation is fully described through

$$\nabla \cdot \kappa_\mathrm{e} \nabla (T_\mathrm{e} - T_0) - g(T_\mathrm{e} - T_0) \approx -p^\mathrm{abs}, \qquad (1)$$

where p^abs is the power density of optical absorption. Further assuming a constant value of κ_e, this equation allows us to obtain a characteristic electronic-heat-diffusion distance $D_\mathrm{e} = \sqrt{\kappa_\mathrm{e}/g}$. Indeed, a measure of the degree of heat localization is provided by the electron temperature profile produced by a line heat source, $T_\mathrm{e}(x) \propto \mathrm{e}^{-|x|/D_\mathrm{e}}$, as a function of distance x to it. Under the conditions of Figs. 1 and 2, we have $D_\mathrm{e} \approx 293\,\mathrm{nm} \sim W$, which explains why T_e is nearly uniform across the ribbon, unlike the cosine-like p^abs transversal profile associated with the dipolar plasmon under consideration (see Fig. S6 in SM [43]). The uniformity of T_e now allows us to write the analytical estimate $T_\mathrm{e} = T_0 + I^\mathrm{inc}(\sigma^\mathrm{abs}/\mathrm{Area})/g$ for clean graphene, represented in Fig. 2(b) [symbols, with $\sigma^\mathrm{abs}/\mathrm{Area}$ taken at the peak frequencies of Fig. 2(a)], in excellent agreement with full numerical simulations (solid blue curve).

Incidentally, the values of the relaxation time τ and the out-of-plane thermal conductance G, which depend on both the material quality and the properties of the surrounding media, affect T_e and T_l: they increase with decreasing G, while the opposite behavior is observed for decreasing optical damping τ^{-1} (see Fig. S4 in SM [43]). Nevertheless, the influence of G is minor under the conditions here considered because $T_\mathrm{l} \approx T_0$.

Plasmon confinement in graphene has so far been achieved through lateral patterning (e.g., in ribbons [23, 28]), inhomogeneous doping [60], or nanostructured dielectric environments [61, 62]. These approaches require the use of nanolithography, which is generally detrimental for the graphene quality. Motivated by the above study for graphene ribbons, we explore next a radically different method for producing and actively tuning plasmon confinement in extended, unpatterned graphene that does not require nanostructuring: spatially modulated optical heating can be applied by projecting an on-demand pump pattern, thus configuring an inhomogeneous graphene optical response capable of trapping plasmons and molding their spatial profiles with a resolution limited by far-field diffraction to roughly half the pump wavelength $\lambda_\mathrm{pump}/2$.

We demonstrate the feasibility of this concept by considering an extended clean graphene sheet ($E_\mathrm{F} = 0.3\,\mathrm{eV}$ doping, supported on a substrate ϵ_h), on which a pump *light grating* is formed by interfering two coherent s-polarized CW plane waves ($\lambda_\mathrm{pump} = 785\,\mathrm{nm}$, intensity $I_\mathrm{pump} = 5 - 160\,\mathrm{GW/m^2}$ each, incidence angles

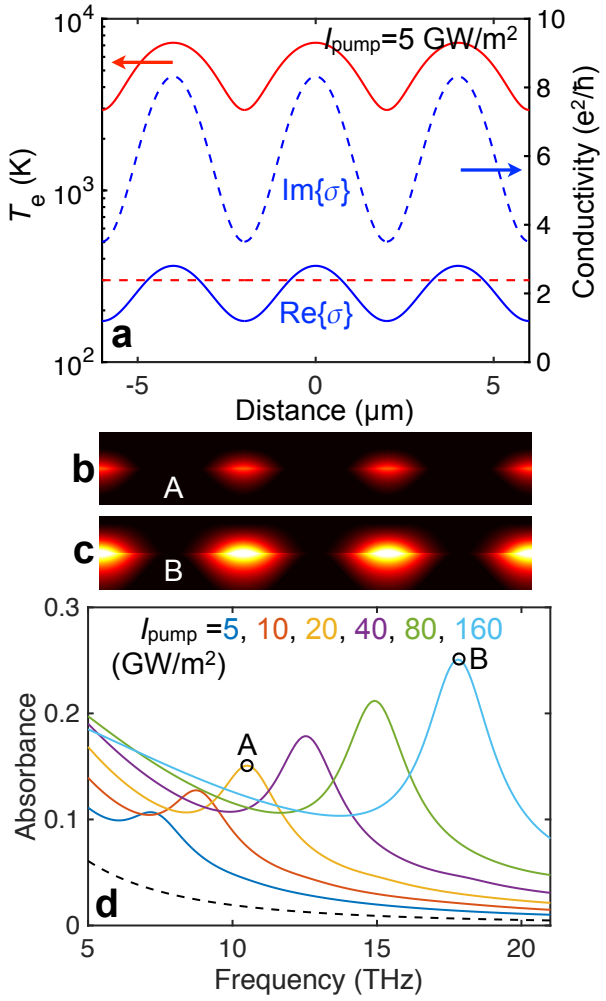

FIG. 3: Photothermal patterning of the optical response of homogeneous graphene. We consider an extended doped clean graphene sheet ($E_F = 0.3\,$eV, $g = 1.21 \times 10^4\,$W/m^{2}K, substrate $\epsilon_h = 4.4$) exposed to a light intensity grating of $4\,\mu$m period, formed by the interference of two CW 785 nm pump plane waves of equal intensity (I_{pump} each). (a) Spatial variation of the self-consistent electron temperature produced by the pump with $I_{pump} = 5\,$GW/m^2 (red solid curve, left scale) and resulting optical conductivity in the local-RPA model (blue curves, right scale) at a probing frequency of 7.2 THz. The ambient temperature level (300 K) is shown for reference (red broken line). (b,c) Near-field intensity plots in a plane transversal to the graphene at the peak plasmon frequencies shown in (d) for $I_{pump} = 20\,$GW/m^2 (A) and 160 GW/m^2 (B). (d) Absorption spectra probed in the THz region with (solid curves) and without (dashed curve) light grating pumping for various values of I_{pump}.

$\pm\theta = \pm 5.6°$). The in-plane electric-field pump intensity is then $4I_{pump}\cos^2[2\pi \sin\theta(x/\lambda_{pump})]$, where we take the beam directions to lie on the plane formed by the surface normal and the in-plane x axis. Incidentally, we obtain a graphene absorbance $(4\pi \mathrm{Im}\{\sigma\}/c)|t_s|^2 \sim 0.002 - 0.008$ from the local-RPA conductivity σ, with $t_s \approx 2/(1+\sqrt{\epsilon_h})$. This result deviates from the $T_e = 0$ behavior [63, 64] $\approx 0.023\,t_s^2$: thermal smearing of graphene interband transitions causes a reduction in the absorption of visible light (i.e., graphene saturable absorption [65]) over the range of I_{pump} under consideration (see also Figs. S7 and S9 in SM [43]). The resulting self-consistent electron temperature T_e reaches high values ($\sim 7200\,$K for $5\,$GW/m^2) and displays a periodic pattern with a max-to-min contrast ratio ~ 2.5 [Fig. 3(a)]. This imparts a periodic pattern on the optical conductivity, effectively transforming the optical response of the extended graphene layer into that of a graphene ribbon array, which can be also regarded as a thermally imprinted grating. When examining the absorption spectra as a function of probe frequency in the THz region [Fig. 3(d), for normal incidence and probe polarization across the ribbons], a prominent resonance peak is observed, shifting up in frequency as the pump intensity is increased. Interestingly, the resonant near-field probe intensity distribution [Fig. 3(b,c)] reveals plasmon confinement in the minima of T_e regions, where $\mathrm{Re}\{\sigma\}$ reaches a minimum (i.e., low inelastic losses), while $\mathrm{Im}\{\sigma\}$ is also minimum and configures an effective plasmon potential well. The depth of such potential well can be estimated through $\max(\mathrm{Im}\{\sigma\})/\min(\mathrm{Im}\{\sigma\})$, a larger value of which indicates a more confining well (see Fig. S9). Also, the quality factor of the resonance [$\sim \mathrm{Im}\{\sigma\}/\mathrm{Re}\{\sigma\}$] increases when raising the pump intensity, as observed in Fig. 3(d) (see also Fig. S9 [43]). When moving to oblique incidence, the plasmons display a characteristic ribbon band dispersion (see SM [43]).

Incidentally, in the design of photothermal modulation we need to reduce the electronic-heat diffusion distance below the characteristic pattern distance (e.g., the optical grating period, $\gg D_e \approx 638\,$nm under the conditions of Fig. 3; see Fig. S8 in SM [43]).

In summary, we have shown that the characteristic weak electron-phonon coupling in clean graphene allows us to reach high electron temperatures well above the lattice temperature, which in turn stays near ambient levels under CW illumination conditions. This produces strong photothermal modulation in the graphene optical response, which we exploit to predict large plasmon shifts in ribbons. We further postulate this effect as an efficient way of dynamically imprinting a spatial modulation of the optical response in extended homogeneous graphene, whereby a spatially patterned optical pump is used to locally heat graphene electrons, thus tailoring an on-demand nanoscale response. We illustrate this concept by showing resonant absorption in a photothermally imprinted grating, whose plasmons can couple to far-field radiation, unlike those of homogenous graphene. Besides circumventing the requirement of nanostructuring, this approach can potentially enable fast plasmon modulation relying on the ability to shape the light pumping beams.

This work has been supported in part by the Spanish MINECO (MAT2017-88492-R and SEV2015-0522),

the European Commission (Graphene Flagship 696656), AGAUR (2014-SGR-1400), Catalan CERCA Program, Fundació Privada Cellex, US National Science Foundation CAREER Award (1552461).

* Corresponding author: javier.garciadeabajo@nanophotonics.es

[1] G. Baffou, R. Quidant, and F. J. García de Abajo, ACS Nano **4**, 709 (2010).

[2] G. Baffou, *Thermoplasmonics: Heating Metal Nanoparticles Using Light* (Cambridge University Press, Cambridge, 2017).

[3] L. Meng, R. Yu, M. Qiu, and F. J. García de Abajo, ACS Nano **11**, 7915 (2017).

[4] A. M. Gobin, M. H. Lee, N. J. Halas, W. D. James, R. A. Drezek, and J. L. West, Nano Lett. **7**, 1929 (2007).

[5] P. K. Jain, I. H. El-Sayed, and M. A. El-Sayed, Nano Today **2**, 18 (2007).

[6] W. Zhao and J. M. Karp, Nat. Mater. **8**, 453 (2009).

[7] M. A. Barral and A. M. Llois, Science **297**, 1160 (2002).

[8] S. Berciaud, D. Lasne, G. A. Blab, L. Cognet, and B. Lounis, Phys. Rev. B **73**, 045424 (2006).

[9] H. M. Pollock and A. Hammiche, J. Phys. D: Appl. Phys. **34**, R23 (2001).

[10] L. Wang and B. Li, Phys. Rev. Lett. **101**, 267203 (2008).

[11] C. Clavero, Nat. Photon. **8**, 95 (2014).

[12] B. Wunsch, T. Stauber, F. Sols, and F. Guinea, New J. Phys. **8**, 318 (2006).

[13] L. Brey and H. A. Fertig, Phys. Rev. B **75**, 125434 (2007).

[14] E. H. Hwang and S. Das Sarma, Phys. Rev. B **75**, 205418 (2007).

[15] M. Jablan, H. Buljan, and M. Soljačić, Phys. Rev. B **80**, 245435 (2009).

[16] Z. Fei, G. O. Andreev, W. Bao, L. M. Zhang, A. S. McLeod, C. Wang, M. K. Stewart, Z. Zhao, G. Dominguez, M. Thiemens, et al., Nano Lett. **11**, 4701 (2011).

[17] L. Ju, B. Geng, J. Horng, C. Girit, M. Martin, Z. Hao, H. A. Bechtel, X. Liang, A. Zettl, Y. R. Shen, et al., Nat. Nanotech. **6**, 630 (2011).

[18] F. H. L. Koppens, D. E. Chang, and F. J. García de Abajo, Nano Lett. **11**, 3370 (2011).

[19] J. Chen, M. Badioli, P. Alonso-González, S. Thongrattanasiri, F. Huth, J. Osmond, M. Spasenović, A. Centeno, A. Pesquera, P. Godignon, et al., Nature **487**, 77 (2012).

[20] Z. Fei, A. S. Rodin, G. O. Andreev, W. Bao, A. S. McLeod, M. Wagner, L. M. Zhang, Z. Zhao, M. Thiemens, G. Dominguez, et al., Nature **487**, 82 (2012).

[21] H. Yan, X. Li, B. Chandra, G. Tulevski, Y. Wu, M. Freitag, W. Zhu, P. Avouris, and F. Xia, Nat. Nanotech. **7**, 330 (2012).

[22] H. Yan, Z. Li, X. Li, W. Zhu, P. Avouris, and F. Xia, Nano Lett. **12**, 3766 (2012).

[23] V. W. Brar, M. S. Jang, M. Sherrott, J. J. Lopez, and H. A. Atwater, Nano Lett. **13**, 2541 (2013).

[24] R. Yu, R. Alaee, F. Lederer, and C. Rockstuhl, Phys. Rev. B **90**, 085409 (2014).

[25] F. J. García de Abajo, ACS Photon. **1**, 135 (2014).

[26] S. Thongrattanasiri, F. H. L. Koppens, and F. J. García de Abajo, Phys. Rev. Lett. **108**, 047401 (2012).

[27] R. Alaee, M. Farhat, C. Rockstuhl, and F. Lederer, Opt. Express **20**, 28017 (2012).

[28] M. S. Jang, V. W. Brar, M. C. Sherrott, J. J. Lopez, L. Kim, S. Kim, M. Choi, and H. A. Atwater, Phys. Rev. B **90**, 165409 (2014).

[29] S. Kim, M. S. Jang, V. W. Brar, K. W. Mauser, L. Kim, and H. A. Atwater, Nano Lett. **18**, 971 (2018).

[30] M. Freitag, T. Low, W. Zhu, H. Yan, F. Xia, and P. Avouris, Nat. Commun. **4**, 1951 (2013).

[31] R. Yu and F. J. García de Abajo, ACS Nano **10**, 8045 (2016).

[32] M. B. Lundeberg, Y. Gao, A. Woessner, C. Tan, P. Alonso-González, K. Watanabe, T. Taniguchi, J. Hone, R. Hillenbrand, and F. H. L. Koppens, Nat. Mater. **16**, 204 (2016).

[33] I. J. Luxmoore, P. Q. Liu, P. Li, J. Faist, and G. R. Nash, ACS Photon. **3**, 936 (2016).

[34] D. Rodrigo, O. Limaj, D. Janner, D. Etezadi, F. J. García de Abajo, V. Pruneri, and H. Altug, Science **349**, 165 (2015).

[35] R. Yu, J. D. Cox, and F. J. García de Abajo, Phys. Rev. Lett. **117**, 123904 (2016).

[36] H. Hu, X. Yang, F. Zhai, D. Hu, R. Liu, K. Liu, Z. Sun, and Q. Dai, Nat. Commun. **7**, 12334 (2016).

[37] G. X. Ni, L. Wang, M. D. Goldflam, M. Wagner, Z. Fei, A. S. McLeod, M. K. Liu, F. Keilmann, B. Özyilmaz, A. H. C. Neto, et al., Nat. Photon. **10**, 244 (2016).

[38] R. Yu, A. Manjavacas, and F. J. García de Abajo, Nat. Commun. **8**, 2 (2017).

[39] I. Gierz, J. C. Petersen, M. Mitrano, C. Cacho, I. C. E. Turcu, E. Springate, A. Stöhr, A. Köhler, U. Starke, and A. Cavalleri, Nat. Mater **12**, 1119 (2013).

[40] V. P. Gusynin, S. G. Sharapov, and J. P. Carbotte, New J. Phys. **11**, 095013 (2009).

[41] R. Yu, J. D. Cox, J. R. M. Saavedra, and F. J. García de Abajo, ACS Photon. **4**, 3106 (2017).

[42] P. Grua, J. P. Morreeuw, H. Bercegol, G. Jonusauskas, and F. Vallée, Phys. Rev. B **68**, 035424 (2003).

[43] See Supplemental Material at http://link.aps.org/supplemental/...

[44] J. K. Viljas and T. T. Heikkilä, Phys. Rev. B **81**, 245404 (2010).

[45] J. C. W. Song, M. Y. Reizer, and L. S. Levitov, Phys. Rev. Lett. **109**, 106602 (2012).

[46] A. Betz, S. H. Jhang, E. Pallecchi, R. Ferreira, G. Fève, J.-M. Berroir, and B. Plaçais, Nat. Phys. **9**, 109 (2013).

[47] M. W. Graham, S.-F. Shi, D. C. Ralph, J. Park, and P. L. McEuen, Nat. Phys. **9**, 103 (2013).

[48] C. B. McKitterick, D. E. Prober, and M. J. Rooks, Phys. Rev. B **93**, 075410 (2016).

[49] T. Low, V. Perebeinos, R. Kim, M. Freitag, and P. Avouris, Phys. Rev. B **86**, 045413 (2012).

[50] M. Freitag, T. Low, and P. Avouris, Nano Lett. **13**, 1644 (2013).

[51] K.-J. Tielrooij, N. C. Hesp, A. Principi, M. B. Lundeberg, E. A. Pogna, L. Banszerus, Z. Mics, M. Massicotte, P. Schmidt, D. Davydovskaya, et al., Nat. Nanotech. **13**, 1 (2017).

[52] S. Yiğen, V. Tayari, J. O. Island, J. M. Porter, and A. R. Champagne, Phys. Rev. B **87**, 241411 (2013).

[53] J. Crossno, J. K. Shi, K. Wang, X. Liu, A. Harzheim, A. Lucas, S. Sachdev, P. Kim, T. Taniguchi, K. Watanabe, et al., Science **351**, 1058 (2016).

[54] T. Y. Kim, C.-H. Park, and N. Marzari, Nano Lett. **16**, 2439 (2016).
[55] X. Du, I. Skachko, A. Barker, and E. Y. Andrei, Nat. Nanotech. **3**, 491 (2008).
[56] L. Wang, I. Meric, P. Y. Huang, Q. Gao, Y. Gao, H. Tran, T. Taniguchi, K. Watanabe, L. M. Campos, D. A. Muller, et al., Science **342**, 614 (2013).
[57] M. M. Jadidi, J. C. König-Otto, S. Winnerl, A. B. Sushkov, H. D. Drew, T. E. Murphy, and M. Mittendorff, Nano Lett. **16**, 2734 (2016).
[58] F. J. García de Abajo, ACS Nano **7**, 11409 (2013).
[59] J. D. Cox, R. Yu, and F. J. García de Abajo, Phys. Rev. B **96**, 045442 (2017).
[60] M. B. Rhouma, M. Oueslati, and B. Guizal, Superlattices and Microstructures **96**, 212 (2016).
[61] W. Gao, G. Shi, Z. Jin, J. Shu, Q. Zhang, R. Vajtai, P. M. Ajayan, J. Kono, and Q. Xu, Nano Lett. **13**, 3698 (2013).
[62] X. Zhu, W. Yan, P. Uhd Jepsen, O. Hansen, N. Asger Mortensen, and S. Xiao, Appl. Phys. Lett. **102**, 131101 (2013).
[63] K. F. Mak, M. Y. Sfeir, Y. Wu, C. H. Lui, J. A. Misewich, and T. F. Heinz, Phys. Rev. Lett. **101**, 196405 (2008).
[64] R. R. Nair, P. Blake, A. N. Grigorenko, K. S. Novoselov, T. J. Booth, T. Stauber, N. M. R. Peres, and A. K. Geim, Science **320**, 1308 (2008).
[65] A. Marini, J. D. Cox, and F. J. García de Abajo, Phys. Rev. B **95**, 125408 (2017).